Hyperfine interactions at ^{57}Fe in Fe^{2+}-doped $MnCO_3$

D. C. Price,* I. Maartense, and A. H. Morrish
Department of Physics, University of Manitoba, Winnipeg, Canada
(Received 3 July 1973)

Mössbauer spectroscopy has been used to determine the magnetic state of Fe^{2+} ions that have been substituted for Mn^{2+} in $MnCO_3$ for temperatures between 1.8 °K and the Néel temperature ($\sim$ 35 °K). Iron concentrations up to 10 mole % have been examined. Within these ranges, the ^{57}Fe Mössbauer spectra show marked dependence on both iron content and temperature. The results have been interpreted in terms of the interactions between the magnetic crystal and a single ferrous ion, and support a model proposed recently for this system in which the Mn^{2+} spins are reoriented in the presence of the ferrous ions due to their large single-ion anisotropy in the trigonal crystal field.

I. INTRODUCTION

It has been shown by magnetization and susceptibility measurements[1,2] that dilute solutions of $FeCO_3$ in $MnCO_3$ have interesting magnetic properties. Both pure materials crystallize with very similar rhombohedral structures[3] and in both there exist exchange interactions that lead to antiferromagnetic ordering below $T_N \approx 35$ °K. In pure $MnCO_3$, the predominant anisotropy energy is due to dipolar interactions. This is relatively weak and favors the basal plane for the Mn^{2+} spin direction, thus allowing a weak ferromagnetic moment to occur through the presence of an antisymmetric exchange interaction.[4] It was found in Ref. 2 (hereinafter referred to as I) that this weak moment decreases rapidly when $MnCO_3$ is doped with Fe^{2+}, being effectively absent for concentrations above 3.5 mole% of $FeCO_3$. This was interpreted as a rotation of the Mn^{2+}-spin direction toward the crystal c axis so that the antisymmetric exchange is no longer allowed. The origin of this spin reorientation lies in the large single-ion anisotropy of the ferrous ion, which is the result of the combined effects of the trigonal crystal field and spin-orbit coupling on the ^5D ground state, and which favors the c axis for the Fe^{2+} spin direction. Competition between the Mn^{2+} anisotropy and Mn-Fe exchange energies leads to the rotation of the Mn spins. Within the Fe^{2+}-doping range where this reorientation takes place, the presence of a thermoremanent offset moment suggests that the Mn^{2+} and Fe^{2+} spin directions are not collinear.

In the work reported here we have measured the hyperfine interactions at the iron sites using Mössbauer spectroscopy, and from these measurements we deduce the properties of the solute ferrous ions as functions of doping concentration and temperature.

Mössbauer spectroscopy allows measurement of the three leading terms in the multipole expansion of the hyperfine-interaction energy between an atomic nucleus and its surrounding electrons. These are the electric monopole, magnetic dipole, and electric quadrupole terms. While each term contains the product of a nuclear and an electronic quantity, the properties of the ^{57}Fe nucleus involved in the interactions mentioned above are considered to be sufficiently well known that information regarding the electronic distribution in the ferrous ion can be deduced. This information is characterized by the electronic charge density at the nuclear site, the magnetic hyperfine field and the electric field gradient at the nuclear site, and because they are properties of a distribution evaluated at a single point they cannot be unambiguously interpreted without some prior knowledge of the electronic state of the ferrous ion in manganese carbonate.

In Sec. II, implicity using the results of a variety of experiments, we describe a model from which the electronic structure of the ferrous ion in its present environment can be determined, and in Sec. III show how the properties measured by Mössbauer experiments are derived. From measurements at low temperatures (≤ 4.2 °K) on samples containing different concentrations of iron it proved to be possible to deduce all the information required for the description of the state of the ferrous ion, and this is done in Sec. IV; the results and some of their implications are discussed in Sec. V. A simple extension to the model to describe the temperature dependence of the Fe^{2+} wave functions with no free parameters is proposed (Sec. VI) and the relevant measurements are discussed in terms of it in Sec. VII.

II. Fe^{2+} ION IN $MnCO_3$ ($T = 0$)

We will assume that the ferrous ion is situated in a crystalline electric field of trigonal symmetry produced by the host $MnCO_3$ lattice. The electronic state of Fe^{2+} in a field of this symmetry has been discussed before,[5] and has been related to susceptibility and magnetization measurements

We assume that the crystal field is much weaker than intra-atomic Coulomb interactions, so that the ^5D ground state of the free-ion $3d^6$ configuration is perturbed by a potential considered to be the sum of a large component with cubic symmetry and a smaller trigonal component. We then make the approximation that the cubic component of this potential is much larger than all other perturbations, so that the ground state in the cubic field (an orbital triplet) may be used to calculate the states resulting from the presence of the trigonal field component, spin-orbit coupling and exchange with the ion's magnetic neighbors. The empirical justification of this approach is that the splitting due to the trigonal field is $\sim 10^3$ cm^{-1} while the cubic potential term splits the ^5D state into two levels separated by $\sim 10^4$ cm^{-1}; nevertheless there are indications that some errors may be introduced.[6]

The cubic states are an orbital triplet with T_{2g} symmetry (the ground state) and an orbital doublet (E_g). The angular parts of the T_{2g} orbital functions, which are to be used as basis functions, may be written in the trigonal coordinate system as[7]

$$\psi_0 = Y_2^0,$$
$$\psi_{+1} = (\sqrt{\tfrac{2}{3}})\, Y_2^{-2} + (\sqrt{\tfrac{1}{3}})\, Y_2^1 , \qquad (1)$$
$$\psi_{-1} = (\sqrt{\tfrac{2}{3}})\, Y_2^2 - (\sqrt{\tfrac{1}{3}})\, Y_2^{-1},$$

where $Y_l^m(\theta, \phi)$ are spherical harmonics of order l. The quantization z axis is the trigonal c axis ($\theta = 0$), a cubic [111] direction. For interactions within the T_{2g} orbitals only, these three functions behave like eigenfunctions of an angular momentum operator $\vec{l}$ with $l = 1$. This is referred to as the T_{2g}-p equivalence.[8] The suffixes on the functions [Eq. (1)] are the eigenvalues l_z of this pseudoangular momentum.

When the ionic ground-state spin $S = 2$ is taken into account, the T_{2g} level has a degeneracy of 15. These 15 spin orbitals are denoted by $\Psi_k = \psi_i \chi_j$ ($i = 0, \pm 1$; $j = 0, \pm 1, \pm 2$) where χ_{m_s} are the five spin functions of $S = 2$. Within this representation we wish to find the eigenfunctions and eigenvalues of the perturbation Hamiltonian

$$\mathcal{H}' = \mathcal{H}_{trig} + \mathcal{H}_{so} + \mathcal{H}_{ex} . \qquad (2)$$

The energy levels resulting from progressively switching on these interactions are shown in Fig. 1, for the simple case of an exchange interaction causing spin ordering along the trigonal axis, as occurs in $FeCO_3$. Evaluation of the terms in $\mathcal{H}'$, allowing for nonaxial directions of the exchange, is described below.

A. Trigonal crystal field – $\mathcal{H}_{trig}$

The second-order axial component of the crystal field can be represented by a potential that can be written in Cartesian coordinates as[7] $V_{trig} \propto 3z^2 - r^2$. The matrix elements of this potential can

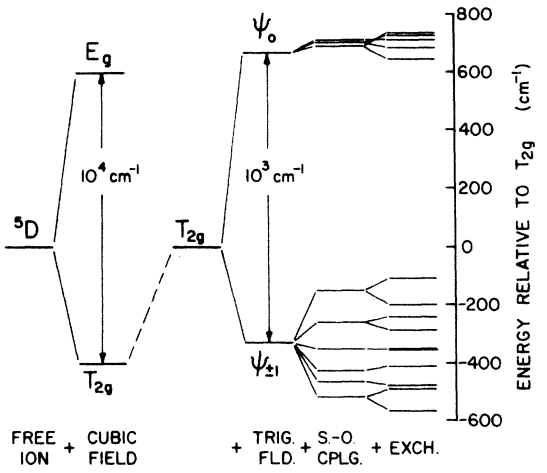

FIG. 1. Energy-level scheme for the free ferrous ion under the action of the cubic and trigonal crystal fields plus spin-orbit coupling plus exchange parallel to the trigonal axis.

be evaluated by means of the operator equivalent technique,[7,9] and give

$$\mathcal{H}_{trig} \propto 3L_z^2 - L(L+1) = \Delta[L_z^2 - \tfrac{1}{3}L(L+1)] . \qquad (3)$$

The parameter Δ determines the separation between the orbital doublet ($\psi_{\pm 1}$) and the singlet (ψ_0) into which the T_{2g} level is split by the action of V_{trig} alone. Typically observed values of this splitting are $|3\Delta| = 10^3$ cm^{-1} for Fe^{2+} in trigonal environments.[5] Mössbauer quadrupole interaction data[6,10] indicate that the orbital doublet is lowest in $FeCO_3$.

We neglect the effect of any fourth-order terms in the crystal field. Interaction with the cubic E_g level[6] could mix perhaps 5% of the E_g states into the lower doublet, changing the numerical factors in $\psi_{\pm 1}$ [Eq. (1)]. We do not wish to introduce any parameters that do not improve our understanding of the experimental results at present, although inclusion of fourth-order terms is shown to be necessary in some materials.[11]

B. Spin-orbit coupling – $\mathcal{H}_{so}$

The coupling between the total spin and orbital angular momenta has the form $\lambda \vec{L} \cdot \vec{S}$, where the constant λ is taken to be the product of the free-ion value $\lambda_0 = -103$ cm^{-1} and a factor α^2 that accounts for a decrease due to the effect of covalency.[12–14] Thus we write

$$\mathcal{H}_{so} = \lambda \vec{L} \cdot \vec{S} = \alpha^2 \lambda_0 [L_z S_z + \tfrac{1}{2}(L_+ S_- + L_- S_+)] \qquad (4)$$

and we leave α^2 as an adjustable parameter.

C. Magnetic interaction – $\mathcal{H}_{ex}$

We start by considering a simple molecular field model for the exchange interaction, with

$$\mathcal{H}_{ex} = -2\sum_i J_i \vec{S}_i \cdot \vec{S} = \vec{H}_{ex} \cdot \vec{S}, \quad (5)$$

where the effective spin $\vec{S}$ of the Fe^{2+} ion is coupled to the surrounding Mn^{2+} spins $\vec{S}_i$ by an exchange integral J_i. We will restrict the summation to the six nearest neighbors, and assume that the $\vec{S}_i$ of the magnetic host sublattice are collinear. $\vec{H}_{ex} = -2\sum_i J_i \vec{S}_i$ is then taken to be an effective exchange field of magnitude $J'\langle S_i\rangle$ and orientation θ_{ex} with respect to the trigonal axis: θ_{ex} is therefore equivalent to θ_{Mn}, the orientation of the Mn^{2+} spins. The molecular field constant $J' = -2\sum_i J_i$ is expected to have a value somewhat larger than that in pure $MnCO_3$[15] ($J_{Mn\text{-}Mn} \approx -12\,cm^{-1}$) but is left as a parameter to be fitted to the experimental data.

The statistical average spin $\langle S_i\rangle$ of the Mn^{2+} ions will not be a function of θ_{ex} since the S-state ion has spherical symmetry. Use of the Brillouin function of spin $\frac{5}{2}$ to describe the temperature variation of $\langle S_i\rangle$ will lead to inaccuracies, but these will almost certainly be no more serious than those that are inherent in other aspects of the molecular field approximation. The justification for the assumption of collinearity of the Mn^{2+} spins[2] is found in the weakness of spin anisotropy relative to the Mn-Mn exchange, since the main sorce of the anisotropy is the long-range dipolar interaction.[16,17] Thus, all Fe^{2+} impurities should experience an exchange field with the same strength and orientation (ignoring the small number of Fe-Fe nearest-neighbor pairs).

If $\vec{H}_{ex}$ is restricted to the xz plane, imaginary components are eliminated from the Hamiltonian matrix and consequently from the eigenfunctions also (although the ψ_i basis functions are not themselves real). This simplification involves no loss of generality because of the axial symmetry of both the crystal and the basis functions. Then we have

$$\mathcal{H}_{ex} = \vec{H}_{ex} \cdot \vec{S} = J'\langle S_i\rangle (S_z \cos\theta_{ex} + S_x \sin\theta_{ex})$$
$$= J'\langle S_i\rangle [S_z \cos\theta_{ex} + \tfrac{1}{2}(S_+ + S_-)\sin\theta_{ex}]. \quad (6)$$

Only the dominant magnetic interaction is accounted for in this Hamiltonian; considering the approximations up to this point, minor terms such as dipolar interactions with the surrounding spins may be safely neglected.

A problem arises from the use of a constant J' while the Fe^{2+} spin direction changes because the spatial symmetry of the Fe^{2+} wave functions depends on the spin direction through the spin-orbit coupling. When a nonaxial exchange field induces a perpendicular spin component S_x it will at the same time lead to an orbital moment L_x. This is achieved by admixture of the orbital singlet ψ_0 into the ground state; the resulting state has a different spatial symmetry than has the ground state in an axial field, which consists of only the orbital doublet ($\psi_{\pm 1}$) functions. Since the exchange mechanism leading to J' is sensitive to the orbital overlap of neighboring ions, it is to be expected that J' will depend on θ_{ex}, the direction of the exchange field. It should be pointed out that this effect has the same origin as the strong magnetic anisotropy of the Fe^{2+} ion in the carbonate lattice.

We will calculate the eigenfunctions and their eigenvalues assuming a constant J' and examine the consequences later. Diagonalization of the 15×15 matrix $\langle\Psi_k|\mathcal{H}'|\Psi_{k'}\rangle$ will give the energies E_n and the wave functions

$$\Phi_n = \sum_{k=1}^{15} a_{nk}\Psi_k, \quad (7)$$

where the coefficients a_{nk} are real because of the restriction of $\vec{H}_{ex}$ to the xz plane.

III. MÖSSBAUER-EFFECT OBSERVABLES

The purpose of this work is to determine the electronic state of the Fe^{2+} impurities by means of Mössbauer spectroscopy. We can extract from the spectra the value of the magnetic hyperfine field, the electric field gradient at the nucleus, and their relative orientations. We are therefore required to relate these observables to the expectation values of the spin and orbital operators for the states Φ_n obtained in Sec. II. In general we have, for the expectation value $\langle O\rangle$ of the operator O, the ensemble average at temperature T

$$\langle O\rangle = \sum_{n=1}^{15} \langle\Phi_n|O|\Phi_n\rangle e^{-E_n/kT} \Big/ \sum_{n=1}^{15} e^{-E_n/kT}. \quad (8)$$

The calculation of the observable quantities is outlined below. It should be pointed out that values determined in this way will only correspond with measured quantities when the lifetime of the first excited state of the ^{57}Fe nucleus (1.4×10^{-7} sec) is much longer than transition times between the electronic levels, so that the ensemble average [Eq. (8)] is equivalent to a time average. This is not always the case, but it seems unlikely that relaxation effects will be important except perhaps at temperatures close to the Néel point.[10]

A. Effective magnetic field at the nucleus

As enumerated by Marshall and Johnson,[18] the three main contributions to the magnetic hyperfine field $\vec{H}_{hf}$ are as follows, when expressed in terms of the orbital and spin angular momentum operators $\vec{L}$ and $\vec{S}$, the $3d$-electron radial coordinate r, and the Bohr magneton μ_B.

(a) The first contribution is the field produced by the orbital moment of the Fe^{2+} ion,

$$\vec{H}_L = 2\mu_B\langle r^{-3}\rangle\langle\vec{L}\rangle. \quad (9)$$

$\langle\vec{L}\rangle$ is nonzero below T_N because of the combined effects of exchange and spin-orbit coupling. It can be directly related to the spectroscopic split-

ting tensor g.[18,19]

(b) The second contribution is the dipolar field due to the net electronic spin moment of Fe^{2+},

$$\vec{H}_D = -\tfrac{1}{2}\mu_B\langle r^{-3}\rangle\langle(3\vec{S}\cdot\vec{r})\vec{r}/r^2 - \vec{S}\rangle . \quad (10)$$

This field is nonzero only for an aspherical spin density, and is related to the electric field gradient, which arises from an aspherical charge density.[18,19] Evaluation of $\vec{H}_D$ by means of equivalent operators[7,9] gives

$$\vec{H}_D = \tfrac{1}{7}\mu_B\langle r^{-3}\rangle[\tfrac{3}{2}\vec{L}(\vec{L}\cdot\vec{S}) + \tfrac{3}{2}(\vec{L}\cdot\vec{S})\vec{L} - L(L+1)\vec{S}]. \quad (10a)$$

(c) The third contribution is the Fermi contact field, proportional to the electronic spin density at the nucleus,

$$\vec{H}_s = \tfrac{1}{2}H_c\langle\vec{S}\rangle . \quad (11)$$

The contact-term effective field H_c has been calculated to be -550 kOe for the free ion,[20] although a reduction due to the effects of covalency is to be expected. This term arises mainly from the polarization of the inner s electrons by exchange interaction with the $3d$ electrons, and is therefore assumed to be proportional to the net ionic spin $\langle\vec{S}\rangle$.

The hyperfine field is then given by $\vec{H}_{hf} = \vec{H}_L + \vec{H}_D + \vec{H}_s$.

B. Electric field gradient at the nucleus

The most important contribution to the electric field gradient (efg) at the ^{57}Fe nucleus is due to the aspherical charge distribution of the $3d$ electrons in the ferrous ion. The components V_{ij} of the efg tensor,[13,21] when evaluated by operator equivalents, are related to the same orbital operators as the dipolar field $\vec{H}_D$, as remarked above. In fact, when the orbital states ψ_i are not mixed (i.e., when $\lambda = 0$), the efg tensor reduces to a vector proportional to $\vec{H}_D$.[18,22] When the efg tensor is rotated to its principal axes,[13,21] the coupling constant for the quadrupole interaction is defined as $\Delta E = \tfrac{1}{4}eQV'_{zz}$, where V'_{zz} is the maximum component of the gradient, e is the electronic charge, and Q is the quadrupole moment of the first excited state ($I = \frac{3}{2}$) of the ^{57}Fe nucleus; the nuclear ground state has spin $I = \frac{1}{2}$ and therefore no quadrupole moment. The remaining principal components of the efg may be described by an asymmetry parameter $\eta = (V'_{xx} - V'_{yy})/V'_{zz}$ because $\vec{V}'$ satisfies the Laplace equation.

Analysis of the observed spectra will give the direction of $\vec{H}_{hf}$ in terms of the polar and azimuthal angles θ'_{hf} and ϕ'_{hf} referred to the principal axes of the efg. In the present case it is found that the z axis of the efg coincides almost exactly with the trigonal crystal axis, and we will henceforth let $\vartheta'_{hf} = \theta_{hf}$. It may be noted here that, in general, the hyperfine field, the effective Fe^{2+} spin direction, and the exchange field are not collinear, i.e., $\theta_{hf} \neq \theta_{Fe} \neq \theta_{ex}$.

Note on use of $\langle r^{-3}\rangle$. In the discussion above, the parameter $\langle r^{-3}\rangle$ has been introduced in the expressions for $\vec{H}_L$ and $\vec{H}_D$ (and $\vec{V}$) but its effect on each of these quantities depends on electronic screening produced by the closed shells in the ionic core, and these effects are not necessarily the same for all the interactions. Strictly speaking, we should define separate parameters $\langle r^{-3}\rangle_L$, $\langle r^{-3}\rangle_D$, and $\langle r^{-3}\rangle_Q$ to account for the different screening mechanisms, but Freeman and Watson[23] did an unrestricted Hartree-Fock calculation of the three parameters for a free Fe^{2+} ion, including radial (but not angular) distortions of the core wave functions, and found that they were the same to within 10%. Moreover, it turned out that for the two magnetic interactions the parameters were almost identical. Although there are other factors to be considered[19] it appears that a single effective $\langle r^{-3}\rangle$ may justifiably be used to describe the orbital and dipolar fields. In fact, we will use a single value of $\langle r^{-3}\rangle$ to describe all three interactions: it only appears as the product $\langle r^{-3}\rangle Q$ in the electric quadrupole interaction, and Q, the nuclear quadrupole moment, is treated as an independent parameter anyway. In any case, relatively little emphasis is placed on the results of electric quadrupole interaction measurements in this paper as there are some aspects of detailed behavior that are not fully understood[14] and on which work is continuing. Discussion in general terms, however, remains valid and is included for the sake of completeness.

Johnson[19,22] points out that covalency will cause a reduction of $\langle r^{-3}\rangle$ from its free-ion value. Ingalls[12] and Hazony[14] have also discussed this point.

IV. EXPERIMENTAL DETAILS AND LOW-TEMPERATURE RESULTS

The iron-doped samples of $MnCO_3$ were prepared as described in I, except that iron enriched in ^{57}Fe was used. In addition, the slightly acidified starting solution containing the Mn and Fe ions was passed through a column of Zn-Hg amalgam to ensure that the iron was reduced to the ferrous state. A conventional electromechanically driven Mössbauer spectrometer was used in conjunction with a variable-temperature cryostat in order to obtain spectra of the carbonate samples between 1.8 and 300 °K in zero applied magnetic field. The source of the 14.4-keV γ radiation was ^{57}Co in chromium, and the velocity scale was calibrated using a thin absorber of natural iron and the data of Preston *et al.*[24] From the relative positions of the iron-absorber peaks, the linearity was determined to be exact to within 0.3%.

Because the samples were randomly oriented

powders, the spectra were fitted by a least-squares procedure to spectra calculated as described by Kündig.[25] The spectra obtained at the lowest temperature used for each sample are shown in Fig. 2. The solid lines are calculated spectra whose parameters are listed in Table I. In all cases, the fitting proved to have effectively no dependence on ϕ_{hf} (the standard deviations calculated for this parameter were generally greater than 360°) and ϕ_{hf} is arbitrarily set equal to zero. This lack of dependence reflects the fact that the efg asymmetry is always small, so that the principal axes V'_{xx} and V'_{yy} are poorly defined.

Table I shows that the parameters that vary most strongly with the molar Fe concentration c are the magnitude of the hyperfine field H_{hf} and its orientation θ_{hf}. In Fig. 3 we plot H_{hf} against θ_{hf} to remove the Fe concentration dependence, which we do not wish to consider at this stage. The solid line was calculated as outlined in Secs. II and III, using the following set of parameters, and by varying θ_{ex}, the orientation of the exchance field:

$$3\Delta = -1000\ \text{cm}^{-1} = -1440\ ^\circ\text{K},$$

$$\lambda = \alpha^2\lambda_0 = 0.86\,\lambda_0 = -88.6\ \text{cm}^{-1} = -128\ ^\circ\text{K},$$

$$J' = -22\ \text{cm}^{-1} = -32\ ^\circ\text{K},$$

$$H_c = -495\ \text{kOe},$$

$$\langle r^{-3}\rangle = 3.91\ \text{a.u.}$$

This set of values is not necessarily the best possible set: The parameters show a certain amount of mutual dependence, and lack of computer time prohibited an exhaustive search of possible combinations of values. The set listed above was chosen after a visual inspection of graphs similar to Fig. 3, although "best" fits for a range of values of the crystal-field parameter appeared to be equally good, and a representative value is given. In view of this it is unreasonable to quote uncertainties in the values, and it should be emphasized that no quantitative conclusion will be drawn from these. We only wish to show that the Mössbauer data can be reasonably interpreted in terms of the model proposed in I.

The line drawn in Fig. 3 corresponds to a range of θ_{ex} from 0° ($\vec{H}_{ex}$ parallel to trigonal axis) to 87° ($\vec{H}_{ex}$ 3° out of basal plane), and the peak occurs at $\theta_{ex} \approx 77°$. The calculated values of H_{hf} and θ_{hf} at $T = 0$ over the range of θ_{ex} are listed in Table II.

Effects of nonferrous iron

In the spectra of the samples with very low iron content, some resonance peaks were observed (most clearly at high temperatures—see Sec. VII) that were not consistent with Fe^{2+} spectra. These resonances were readily separable from the ferrous spectra and their origins are identified as follows.

(a) *Fe^{3+} in the carbonate lattice.* The small peak at −4.2 mm/sec in the $c = 0.002$ spectrum (Fig. 2) was identified as an Fe^{3+} resonance by repeating the spectrum using a larger velocity range. This is shown in Fig. 4, although a different γ source ($Pd^{57}Co$) was used so that all peaks are shifted by 0.34 mm/sec towards the negative velocity end. The arrows mark the positions of the six lines corresponding to the hyperfine field of 540 kOe and an isomer shift of +0.40 mm/sec (relative to $Pd^{57}Co$); both values are typical of ferric spectra. It was further found (see Sec. VII) that the Fe^{2+} and Fe^{3+} spectra showed the same ordering temperatures (to within a few degrees) and it may therefore be assumed that the Fe^{3+} ions are in the carbonate lattice. The Fe^{3+} was presumably formed during the sample preparation, and in this case a certain quantity, rather than a fixed proportion, of the Fe^{2+} might be expected to be oxidized to

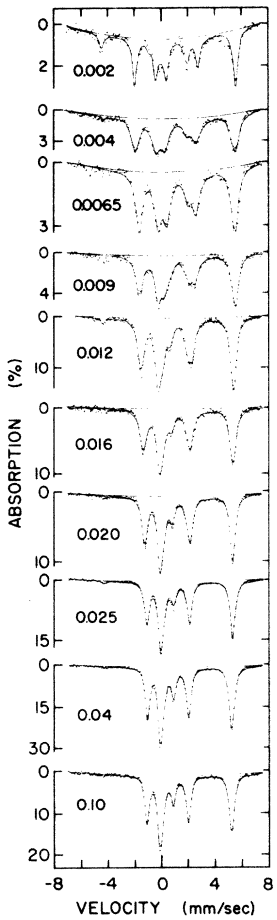

FIG. 2. Mössbauer spectra for the $Mn_{1-c}Fe_cCO_3$ samples at the lowest temperatures employed (see Table I). The drawn curves, which were obtained using the parameters listed in Table I, are explained in the text. The value of c is indicated for each spectrum.

TABLE I. Parameters deduced from the low-temperature Mössbauer spectra. Figures in parentheses represent one standard deviation in the uncertainty in the appropriate quantity.

c (Molar fraction)	T(°K)	H(kOe)	θ_{hf}(deg)	ΔE(mm/sec)	η	δ(mm/sec)[a]
0.002	1.8	194.8 (1.0)	36.0 (0.3)	1.11 (0.02)	0.15 (0.02)	1.582 (0.005)
0.004	4.2	195.2 (0.7)	33.1 (0.3)	1.06 (0.01)	0.07 (0.02)	1.558 (0.005)
0.0065	4.2	184.8 (0.5)	30.2 (0.3)	1.06 (0.01)	0.13 (0.02)	1.529 (0.005)
0.009	4.2	183.9 (0.4)	26.4 (0.3)	1.07 (0.01)	0.08 (0.01)	1.503 (0.004)
0.012	4.2	178.8 (0.2)	21.2 (0.2)	1.04 (0.01)	0.05 (0.01)	1.490 (0.002)
0.016	4.2	173.2 (0.2)	17.4 (0.2)	1.04 (0.01)	0.00 (0.02)	1.499 (0.003)
0.020	4.2	168.9 (0.1)	14.7 (0.1)	1.04 (0.01)	0.06 (0.01)	1.531 (0.001)
0.025	4.2	165.6 (0.05)	7.7 (0.1)	1.03 (0.001)	0.0	1.540 (0.006)
0.040	4.2	162.4 (0.04)	0.0	1.021 (0.001)	0.0	1.531 (0.001)
0.100	4.2	163.1 (0.1)	0.0	1.028 (0.001)	0.0	1.531 (0.001)

[a] δ is the isomer shift measured relative to $Cr^{57}Co$.

Fe^{3+}. The Fe^{3+} spectrum would then be most prominent in the least-doped samples, and this is consistent with the observations.

(b) *Iron impurities in the beryllium windows of the cryostat.* These give a small, broad, unresolved resonance near zero velocity, as was verified by collecting a spectrum with no sample in the cryostat. This resonance was detectable only in the spectra of the $c = 0.002$ and 0.004 samples.

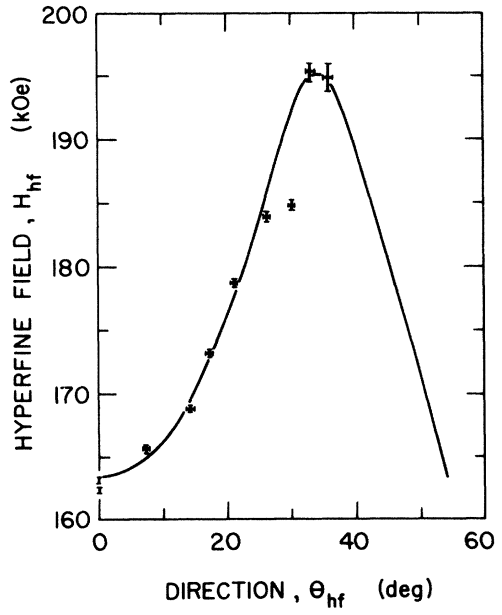

FIG. 3. Magnitude of the ^{57}Fe hyperfine field H_{hf} as a function of its direction θ_{hf} referred to the trigonal axis. The points were obtained from the spectra in Fig. 2; calculation of the curve is explained in Sec. IV.

V. DISCUSSION OF LOW-TEMPERATURE RESULTS

Before discussing those results that are relevant to the magnetic properties of the Fe^{2+} ion, some comments on the values of other parameters obtained from analysis of the spectra are in order. As mentioned in Sec. III, we obtain the product $\langle r^{-3}\rangle Q$ from the electric quadrupole interaction. This interaction was found to be fairly insensitive to iron concentration (see Table I) and the value $\langle r^{-3}\rangle Q = 6.45 \pm 0.20$ a.u. b is obtained. If the effective value of $\langle r^{-3}\rangle$ obtained for the magnetic interactions is used (i.e., $\langle r^{-3}\rangle = 3.91$ a.u.), then the ^{57}Fe nuclear quadrupole moment is $Q = 0.165 \pm 0.005$ b. This agrees well with the value 0.18 b obtained by Johnson,[19,22] even though we have not (Sec. IIIB) taken any account of the small contribution to the quadrupole interaction arising from charges external to the Fe^{2+} ion, which will vary among different materials.

The variation with iron concentration of the asymmetry of the electric field gradient is qualitatively reproduced by the calculations. The efg is axially symmetric (i.e., the asymmetry parameter $\eta = 0$) at the higher doping levels where the exchange field is parallel to the trigonal axis, and as the iron concentration is lowered, η increases with the orbital moment L_x. The calculated asymmetries, however, tend to be smaller than those observed: for $\theta_{ex} = 80°$, which corresponds roughly to the $c = 0.002$ sample, the calculated $\eta = 0.06$, whereas the data show that $\eta = 0.12 \pm 0.02$.

The value of $\alpha^2 = 0.86$ for the covalency factor, which reflects the decrease in the spin-orbit coupling constant λ relative to the free-ion value, is in good agreement with the estimate of $\alpha^2 = 0.9$ made by Okiji and Kanamori[6] for $FeCO_3$. It also falls within the range of 0.6–0.9 reported for various ferrous compounds.[12]

TABLE II. Calculated functions of the state of the Fe^{2+} ion at $T=0$ for various directions of the exchange field, using parameters listed in Sec. IV.

$\theta_{ex}(T=0)$ (deg)	H_{hf} (kOe)	θ_{hf} (deg)	$\langle S_x\rangle$	$\langle S_z\rangle$	$\langle L_x\rangle$	$\langle L_z\rangle$
0.0	163.3	0.0	0.0	1.977	0.0	0.977
10.0	164.3	5.6	0.079	1.975	0.008	0.977
20.0	167.0	11.0	0.156	1.970	0.015	0.976
30.0	171.2	16.0	0.232	1.961	0.022	0.974
40.0	176.5	20.5	0.305	1.949	0.030	0.972
50.0	182.3	24.5	0.375	1.933	0.037	0.969
60.0	188.2	28.0	0.443	1.911	0.044	0.962
65.0	191.0	29.7	0.476	1.897	0.048	0.957
70.0	193.3	31.3	0.510	1.877	0.051	0.949
75.0	194.9	33.3	0.547	1.843	0.056	0.935
80.0	194.3	36.1	0.593	1.770	0.061	0.899
85.0	182.6	43.4	0.668	1.500	0.069	0.763
87.0	166.0	52.1	0.714	1.165	0.074	0.593
90.0	136.1	90.0	0.767	0.000	0.080	0.000

If we make use of the suggestion by Ingalls[12] (with which Hazony[14] disagrees) that covalency reduces $\langle r^{-3}\rangle$ by the same ratio as it decreases λ, then for the magnetic interactions we obtain an effective value $\langle r^{-3}\rangle = 4.55$ a.u. for the free ion. Agreement with the calculations of Freeman and Watson[23] for the Fe^{2+} free ion is very good. The model on which our calculations are based is further supported by the fact that the value we obtain for H_c (−495 kOe) is within the range previously reported for the Fermi contact hyperfine field constant in ferrous compounds. The reduction of 10% from the calculated free-ion value, $H_c = -550$ kOe, [20] is somewhat less than the 14% reduction in λ, but this is not unexpected.[14]

The value $J' = -22$ cm^{-1} for the exchange constant is of some interest. It is almost twice as large as the Mn-Mn exchange constant in $MnCO_3$,[15] and may in fact approach the value for Fe-Fe exchange in $FeCO_3$, although this latter is unknown. This could be regarded as evidence of Fe-Fe clustering in the samples, but the fit of the data over a considerable range of iron concentrations argues against this since the same value of J' was used in all calculations. Furthermore, the hyperfine field of 163 kOe at $\theta_{ex}=0$ (Fig. 3), is somewhat less than that in $FeCO_3$[10] so the existence of small regions of $FeCO_3$ seems unlikely. (Of course there is a nonzero probability of occurrence of iron nearest-neighbor pairs, but at low concentrations this should have little effect on the results.) An unusually large Mn-Fe exchange coupling was also inferred from the rapid rise of the ordering temperature with increased iron doping in I.

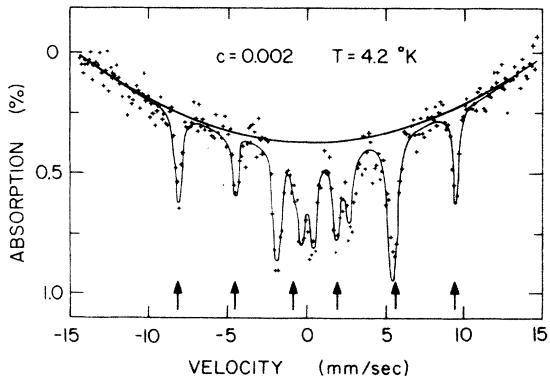

FIG. 4. Mössbauer spectrum of the $c=0.002$ sample at 4.2 °K. The velocity range is larger than that of Fig. 2. The six peaks of the Fe^{3+} spectrum are shown by arrows.

On the basis of the good fit of the calculated curve to the data in Fig. 3, using apparently reasonable values of the various parameters, we conclude that the low-temperature behavior of the Fe^{2+} ions is adequately described by the model in which a system of collinear Mn^{2+} spins produces the same exchange field at all Fe^{2+} ions, and where the orientation, θ_{ex} (= θ_{Mn}), of this field relative to the trigonal axis depends on the Fe^{2+} concentration. We therefore feel justified in using this model as a basis for further discussion of the system.

It is now a simple matter to demonstrate the dependence of the effective spin and orbital angular momenta, $\langle S\rangle\hbar$ and $\langle L\rangle\hbar$, of the Fe^{2+} ion on the direction and strength of the exchange field. The values of $\langle S_x\rangle$, $\langle S_z\rangle$, $\langle L_x\rangle$, and $\langle L_z\rangle$ as functions of θ_{ex} are given in Table II and plotted in Fig. 5(a). The anisotropies of the momenta are further emphasized in Fig. 5(b), where we plot the dependence of $\langle S\rangle$ and $\langle L\rangle$ on the strength of the exchange constant J' for both the parallel and perpendicular orientations of the exchange field, i.e., for θ_{ex}

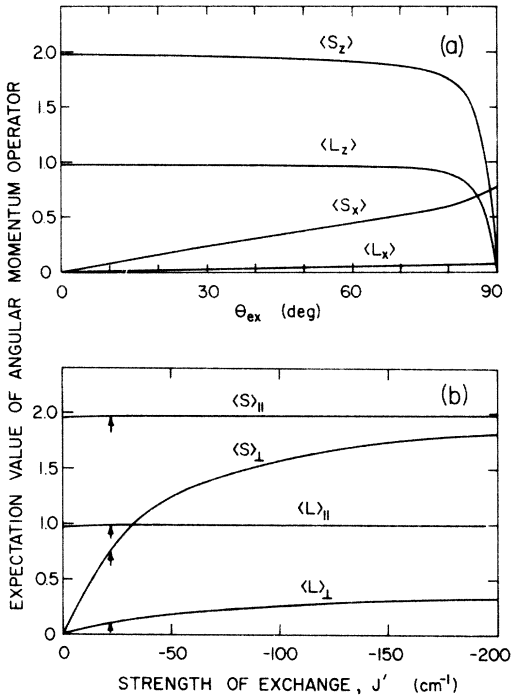

FIG. 5. Expectation values of $\vec{S}$ and $\vec{L}$, the spin and orbital angular momentum operators for the ferrous ion at $T=0$. (a) The x and z components as a function of the exchange field direction θ_{ex} with $J' = -22$ cm^{-1} and (b) as a function of the exchange parameter J', for parallel ($\parallel$) and perpendicular ($\perp$) orientations of the exchange field, referred to the trigonal axis. The arrows indicate the value of J' (-22 cm^{-1}) obtained from the present results.

$= 0°$ and $90°$. These curves are not, of course, unique functions of J', but depend also on the crystal-field splitting Δ and the spin-orbit coupling λ. The strength of the exchange deduced for the system, $J' = -22$ cm^{-1}, is marked in Fig. 5(b). Thus, even at $T=0$, if the exchange field is in the basal plane, neither the full spin nor orbital angular momentum of the Fe^{2+} ion is seen. Full momenta are not developed, in fact, for any nonzero value of θ_{ex} with a finite J', although it is not until $\theta_{ex} \gtrsim 75°$ that the net moment starts to decrease appreciably for our value of J'. This illustrates the strong anisotropy of the susceptibility[5] in $FeCO_3$, as well as the reason why spin flopping is so unfavorable that $FeCO_3$ is metamagnetic.[26]

Figure 5(a) implies that the Mn and Fe spins are not collinear except in the limiting cases where $\theta_{ex} = 0°$ or $90°$. This is consistent with the proposed origin of the thermoremanent offset moment reported in I. With the assumption that $\theta_{Mn} = \theta_{ex}$, Fig. 6(a) shows the direction of the effective Fe^{2+} spin, $\theta_{Fe} = \tan^{-1}(\langle S_x\rangle/\langle S_z\rangle)$, and the difference $\theta_{Mn} - \theta_{Fe}$ as functions of θ_{ex}. While the dependence of these quantities on iron concentration can be estimated from the data in Tables I and II, the value of θ_{ex} for each sample can be more reliably determined from the temperature-dependent results to be presented below. The calculated hyperfine field and spin components in the xz plane are drawn in Fig. 6(b) for three directions of the exchange field.

VI. CALCULATION OF TEMPERATURE DEPENDENCE OF θ_{ex}

If we disregard temperature-dependent changes in the parameters used in the model calculations, then the direction of the exchange field $\theta_{ex}(T)$ is determined by the temperature dependence of the Fe-Mn exchange interaction, since it is this interaction that is responsible for lifting the Mn spin direction out of the basal plane. In a crystal of $MnCO_3$ doped with a molar fraction c of $FeCO_3$, where $\theta_{ex}(T=0)$ is such that $\langle S_x\rangle$ and $\langle S_z\rangle$ are the components of the effective Fe^{2+} spin S at low temperatures, we have for the total energy of the spin system (averaged per ion) at temperature T,

$$E(T) = (1-c)\langle \vec{S}_i\rangle^2 K_{Mn}\cos^2\theta_{Mn}(T) - 2c\sum_i J_i \vec{S}_i \cdot \vec{S}$$
$$= (1-c)\langle \vec{S}_i\rangle^2 K_{Mn}\cos^2\theta_{ex}(T) + cJ'\langle S_i\rangle \times [\langle S_x\rangle \sin\theta_{ex}(T) + \langle S_z\rangle \cos\theta_{ex}(T)]. \quad (12)$$

The first term is the anisotropy energy of the Mn^{2+} spins $\vec{S}_i$, taken to have the form of a magnetic dipolar interaction, with K_{Mn} a constant. The isotropic Mn-Mn exchange is not included because it does not directly affect the temperature dependence of θ_{ex}. Antisymmetric exchange supplies a small energy term favoring the basal plane, but its angular variation is the same as that of the dipolar energy and it may therefore be included in K_{Mn}.

The second term in Eq. (12) is the Fe-Mn exchange energy. As far as other terms are concerned, it should be noted that the Fe^{2+} single-ion anisotropy is implicity accounted for in the determination of $\langle S_x\rangle$ and $\langle S_z\rangle$ and, as before, all other magnetic interactions of the Fe^{2+} ion are considered to have a negligible effect.

The equilibrium value of $\theta_{ex}(T)$ is determined by the condition $\partial E/\partial\theta_{ex} = 0$, so that

$$\frac{(1-c)K_{Mn}}{cJ'} = \frac{1}{2\langle S_i\rangle}\left(\frac{\langle S_x\rangle}{\sin\theta_{ex}(T)} - \frac{\langle S_z\rangle}{\cos\theta_{ex}(T)}\right). \quad (13)$$

The Fe^{2+} spin components have been treated as constants here because the calculation demands an iterative approach: There is no analytic expression for $\langle S_x\rangle$ or $\langle S_z\rangle$ as functions of θ_{ex}, nor for their partial derivatives with respect to θ_{ex}. The energy expression [Eq. (12)] is correct only for the situation where the Mn spin is free to rotate in a field in which the Fe^{2+} spin $\vec{S}$ is fixed, so the

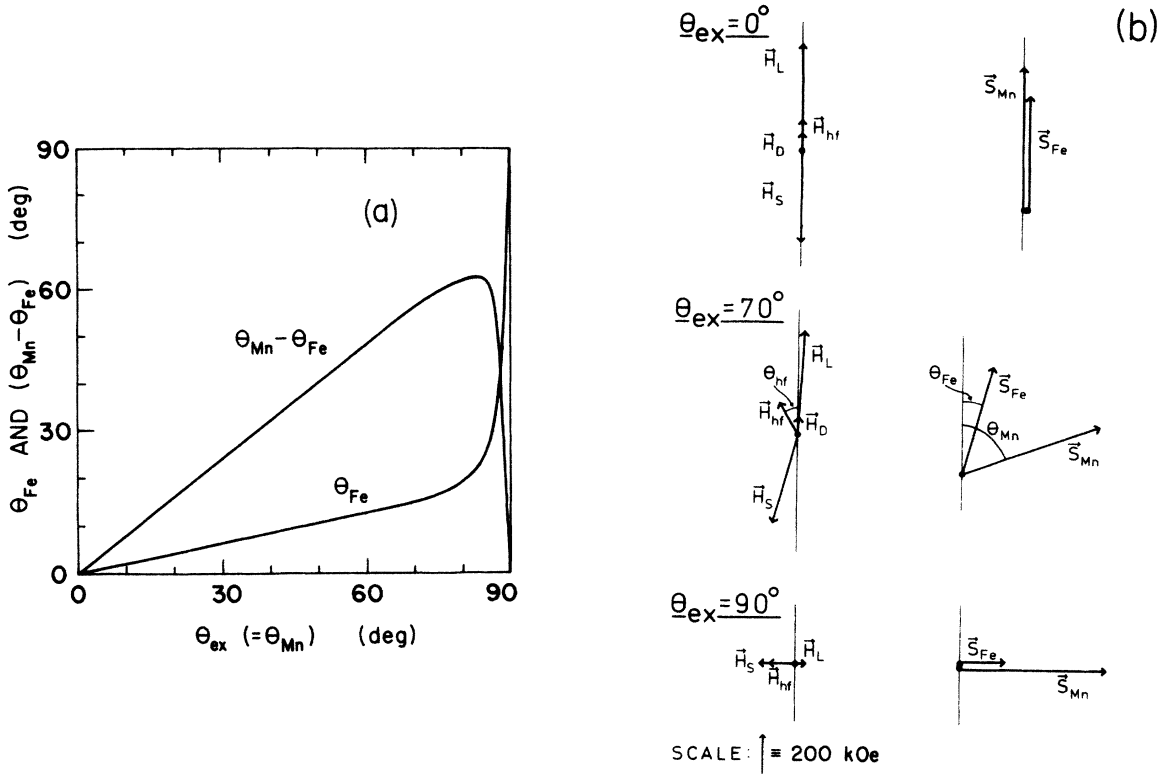

FIG. 6. (a) Effective direction of the ferrous ion spin θ_{Fe} and the difference $(\theta_{Mn}-\theta_{Fe})$ as functions of the direction of the exchange field, $\theta_{ex}=\theta_{Mn}$, with respect to the trigonal axis. (b) Hyperfine field components (left) and effective spin vectors (right) for three directions of the exchange field. The vertical axis represents the crystal c axis.

following procedure was adopted. For a given value of $\theta_{ex}(0)$, $\langle S_x\rangle$ and $\langle S_z\rangle$ are calculated from the eigenfunctions obtained according to Sec. II, and the ratio of (nominal) constants on the left of Eq. (13) is subsequently determined. At temperature T, $\langle\vec{S}_i\rangle$ is found from the Brillouin function of $S=\frac{5}{2}$, and Eq. (13) is solved to find the new value $\theta_{ex}(T)$. Iterations proceed like this until the solutions converge.

The general pattern of behavior of $\theta_{ex}(T)$ depends strikingly on the value of $\theta_{ex}(0)$. For a large $\theta_{ex}(0)$, i.e., for small c, when the Fe-Mn exchange energy is small ($\vec{S}_i\cdot\vec{S}$ small) and the full Fe^{2+} spin $S=2$ is not seen even as $T\to 0$ [see Fig. 5(b)], a rise in temperature has the effect of further weakening the exchange relative to the Mn anisotropy energy, and hence $\theta_{ex}(T)$ increases. This occurs because $\langle\vec{S}\rangle$ decreases with increasing T faster than does $\langle\vec{S}_i\rangle$. The increase in $\theta_{ex}(T)$ is monotonic with T but it occurs mostly over a rather narrow temperature range giving it the appearance of a transition, and this is due to the strong dependence of $\langle S_z\rangle$ on θ_{ex} for larger values of θ_{ex} [Fig. 5(a)]. Examples of this behavior will be given later [Fig. 8(a)].

On the other hand, when $\theta_{ex}(0)$ is small and the Fe-Mn exchange energy is large, $\langle\vec{S}\rangle$ decreases more slowly with increasing T than does $\langle\vec{S}_i\rangle$, and as a result the Mn anisotropy decreases more rapidly than the exchange. This causes a decreasing $\theta_{ex}(T)$ and, again, this effect can be quite rapid. Examples of this will be given in Fig. 8(b).

It is appropriate at this point to recall the limitation in the approximation made in Sec. II C, that the exchange parameter J' is independent of θ_{ex}. This may have significant consequences when $\theta_{ex}(T)$ changes considerably with temperature.

VII. MEASUREMENTS AT HIGHER TEMPERATURES: RESULTS AND DISCUSSION

For each sample, spectra were recorded at a number of temperatures between 4.2 °K and the Néel temperature (~ 35 °K), and were fitted as described in Sec. IV. Two sets of such spectra are shown in Fig. 7: The $c=0.002$ sample spectra are Fig. 7(a) and the $c=0.016$ spectra are Fig. 7(b). The solid lines are the best fits to the spectra.

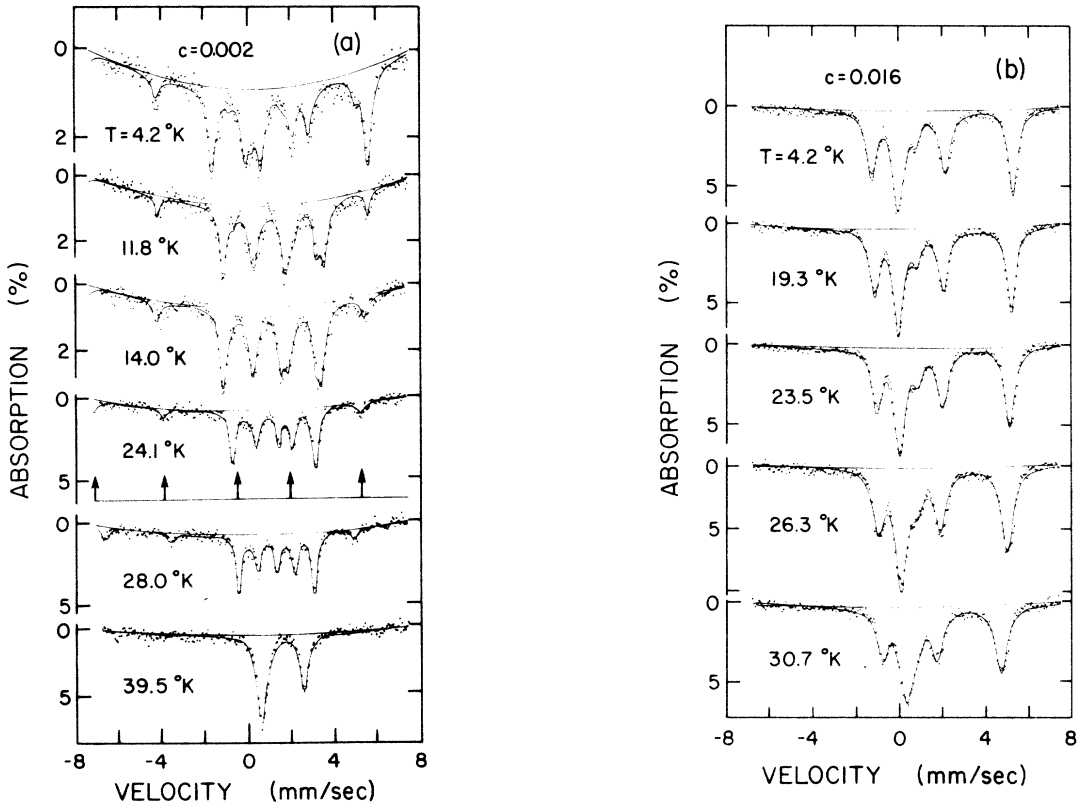

FIG. 7. Mössbauer spectra for two samples of $Mn_{1-c}Fe_cCO_3$ as a function of temperature. The drawn curves, which correspond to the parameters listed in Table III, are explained in Sec. VII. (a) $c = 0.002$ sample. The Fe^{3+} peaks, shown by arrows in the $T = 24.1$ °K spectrum, are evident in all the spectra. They have converged to a single peak by $T = 39.5$ °K. (b) $c = 0.016$ sample.

A. Effects of nonferrous iron

As already remarked (Sec. IV), the presence of Fe^{3+} in the carbonate lattice and iron in the beryllium windows was detected in the spectra of the samples with low iron content. Further information on the Fe^{3+} spectrum was obtained from the temperature dependence of the hyperfine field, which indicated an ordering temperature between 31 °K (where the field was 414 kOe) and 37 °K ($H_{hf} = 0$). We infer that the ferric ions are ordered by the exchange field in the carbonate lattice; other interpretations are possible, but less likely. For all the spectra of the $c = 0.002$ sample, the Fe^{3+} component accounted for $(20 \pm 5)\%$ of the total area (the variation being due to the low signal-to-noise ratio of these spectra) and was correspondingly less intense in the more iron-rich samples. The collapse of the Fe^{2+} spectrum at higher temperatures in the low iron content samples allowed the Fe^{3+} spectrum to be seen more clearly [see Fig. 7(a): the Fe^{3+} peaks are arrowed in the $T = 24.1$ °K spectrum].

B. Ferrous spectra

The variations of the hyperfine field (H_{hf}) and its direction relative to the trigonal axis (θ_{hf}) as functions of temperature for the ferrous spectra in the various samples are listed in Table III. We attempted to reproduce these results by choosing an appropriate value of θ_{ex} ($T = 0$) for each sample and then calculating $\theta_{ex}(T)$ and subsequently $H_{hf}(T)$ and $\theta_{hf}(T)$, using the parameters listed in Sec. IV. Typical results of this procedure are shown in Figs. 8(a) and 8(b), which show two different sorts of behavior of $\theta_{ex}(T)$. The conclusion is that these calculations reproduce the general trend of the results, and we ascribe differences in detail to inadequacies such as the use of single-ion wave functions and a directionally independent molecular-field model, and perhaps also to some inaccuracies in the parameters determined from the low-temperature results.

From this fitting procedure, estimates of the exchange field direction (assumed parallel to the Mn spins) for each sample at low temperatures are

TABLE III. Temperature and concentration dependence of the $^{57}Fe^{2+}$ hyperfine field as deduced from the Mössbauer spectra. Standard deviations in hyperfine field measurements are typically 1 kOe for H_{hf} and 1° for θ_{hf}.

c	T(°K)	H_{hf}(kOe)	θ_{hf}(deg)	c	T(°K)	H_{hf}(kOe)	θ_{hf}(deg)
0.002	1.8	194.8	36.0	0.012	4.2	178.8	21.2
	4.2	186.7	34.9		23.8	158.3	11.9
	11.8	118.8	81.9		29.7	135.2	0.0
	14.0	113.8	84.8				
	19.2	102.2	87.0	0.016	4.2	173.2	17.4
	24.1	89.4	87.2		19.3	166.9	12.6
	28.0	74.9	86.9		23.5	161.1	8.9
					26.3	152.7	3.7
0.004	4.2	195.3	33.1		30.7	135.5	0.0
	16.1	113.5	76.5				
	19.2	103.4	82.1	0.020	4.2	168.9	14.7
	24.8	90.5	88.5		19.8	163.4	7.9
					23.5	159.7	2.0
0.0065	4.2	184.8	30.2		26.8	152.9	0.0
	12.4	174.5	29.4				
	23.5	93.5	78.3	0.025	4.2	165.6	7.7
	28.2	66.0	89.2		19.7	163.9	0.0
					23.4	161.4	0.0
0.009	4.2	183.9	26.4		27.0	154.4	0.0
	16.4	170.5	23.3				
	19.9	162.5	20.8	0.040	4.2	162.4	0.0
	23.2	152.0	18.0		19.9	162.5	0.0
	26.3	141.5	17.8		23.8	160.7	0.0
					27.1	154.6	0.0
					30.4	139.6	0.0

obtained. These are listed in Table IV and plotted in Fig. 9(a). Also listed in Table IV and plotted in Fig. 9(b) is the quantity $(1-c)\sin\theta_{Mn}$. According to Dzyaloshinsky theory,[4] this should be proportional to the weak ferromagnetic moment existing in the Mn spin system, and this moment was measured in I (see Fig. 2 of Ref. 2). It can be seen that the general features are the same (viz., a discontinuity in slope at $c \approx 0.005$ and a rapid decrease of the moment to zero by $c = 0.040$), although for $0.005 < c < 0.040$ the measured moments are smaller than the calculated ones. This may be due either to the inherent inadequacies in the model (in particular to the assumption of a constant J') or to the possibility that, despite the fact that the measured powders were considered to consist of single domain particles, some mechanism prevented the full weak moment from being observed.

It is also observed [Fig. 6(a) of Ref. 2] that for samples in which the doping concentration is greater than about 1 mole% ($c = 0.01$), the weak ferromagnetic moment decreases faster than the sublattice magnetization when T is increased, and this is in accordance with the behavior of $\theta_{ex}(T)$ decreasing towards zero at higher temperatures in these samples. Figure 8(b) contains two examples of this behavior.

The values of the ratio of anisotropy to exchange constants, K_{Mn}/J', derived from the values of θ_{ex} ($T = 0$) [see Eq. (13)], are listed for each concentration in Table IV, and plotted in Fig. 9(c). If the Mn anisotropy energy is due predominantly to dipole-dipole interactions[16,17] then K_{Mn} should be a constant and we must ascribe the variations in the ratio to variations in the exchange parameter J' as $\theta_{ex}(0)$ changes. Reasons for variations such as this have been discussed in Sec. II. It is worth noting that the sort of behavior of J' indicated by Fig. 9(c) can explain qualitatively the differences between calculated and observed $H_{hf}(T)$ curves such as are shown in Fig. 8. For low-concentration samples, such as $c = 0.002$ [Fig. 8(a)], J' would be expected to increase with temperature since $\theta_{ex}(T)$ does. This would lead to larger values of $\langle S_x \rangle$ [see Fig. 5(b)], and consequently larger H_{hf} values at higher temperatures, and this would improve the agreement between calculation and experiment. On the other hand, at higher iron concentrations such as $c = 0.016$ [Fig. 8(b)], $\theta_{ex}(T)$ decreases towards zero as the temperature is raised, so J' would likewise decrease. This would have the effect of making θ_{ex} decrease more slowly (the Mn spins would be less strongly pulled towards the trigonal axis) and therefore $H_{hf}(T)$ and $\theta_{hf}(T)$ would also decrease more slowly, as is required

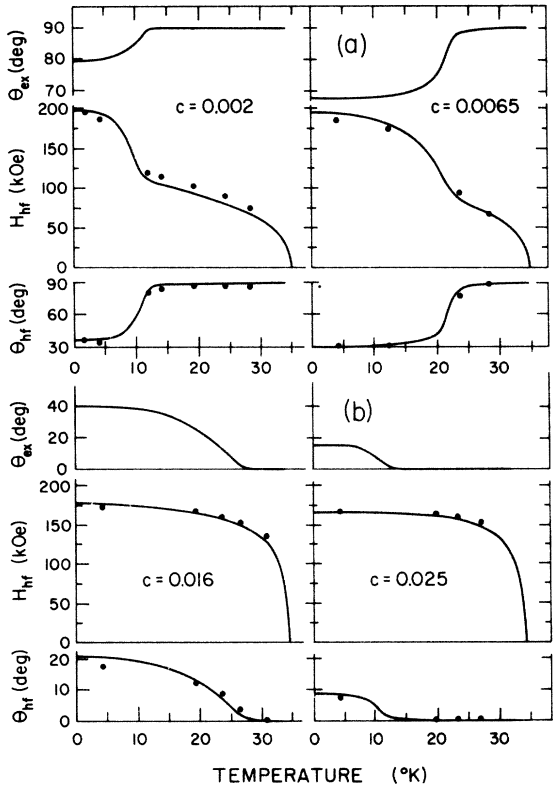

FIG. 8. Exchange-field direction θ_{ex}, the hyperfine field magnitude H_{hf}, and direction θ_{hf} as functions of temperature for four of the samples of $Mn_{1-c}Fe_cCO_3$. The solid curves were obtained as described in Sec. VII using the parameters listed in Sec. IV. (a) $c = 0.002$ and $c = 0.0065$ samples. (b) $c = 0.016$ and $c = 0.025$ samples.

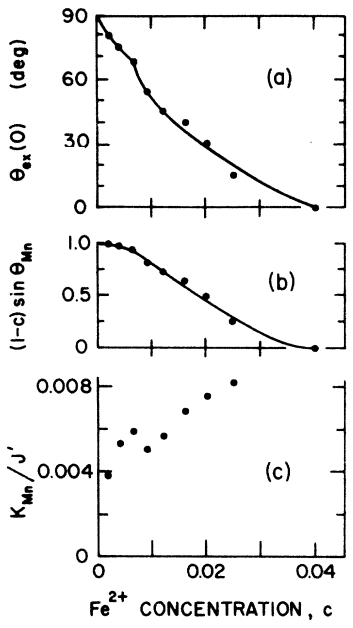

FIG. 9. Some parameters of the exchange field plotted as functions of iron concentration. (a) Direction of the exchange field at $T = 0$, $\theta_{ex}(0)$. (b) $(1-c)\sin\theta_{Mn}$, at $T = 0$, assuming $\theta_{Mn} = \theta_{ex}$. (c) The anisotropy to exchange constant ratio K_{Mn}/J'.

to fit the data in Fig. 8(b).

Finally, we note that the magnitude of the ratio K_{Mn}/J' (~ 0.005) appears to justify the assertion made in Sec. II C that the Mn spin anisotropy is weak relative to the exchange interactions.

VII. CONCLUSION

From the manner in which the present results are reproduced by a simple molecular field model, we conclude that the concept proposed in I of spin reorientation as a function of iron content gives a consistent description of the macroscopic and microscopic magnetic properties of the system that have been measured so far. Although there are some minor discrepancies between experimental and calculated quantities, it is felt that these can be (at least qualitatively) explained in terms of a dependence of the strength of the Fe-Mn exchange coupling constant on the direction of the Mn^{2+} ion spins. Quantitative determination of this dependence, however, would require detailed calculation of orbital overlap.

The results also indicate that, at least for the magnetic interactions, the effect of covalency on the single-ion wave functions can be adequately accounted for by a reduction of quantities such as λ, $\langle r^{-3}\rangle$, and H_c. It is not clear that the effects of covalency on the electric quadrupole interaction can be accounted for so readily,[14] and work is continuing on this aspect of the problem.

There may be interest in further testing some aspects of this model by inducing spin reorientations with applied magnetic fields. As a matter of fact, some Mössbauer effect measurements were carried out at 4.2 °K in applied fields up to 50 kOe

TABLE IV. Fe^{2+} concentration dependence of exchange parameters.

c	$\theta_{ex}(T=0)(=\theta_{Mn})$	$(1-c)\sin\theta_{Mn}$	K_{Mn}/J'
0.002	80°	0.983	0.0038
0.004	75°	0.962	0.0052
0.0065	68°	0.921	0.0059
0.009	54°	0.802	0.0050
0.012	45°	0.699	0.0055
0.016	40°	0.633	0.0068
0.020	30°	0.490	0.0074
0.025	15°	0.253	0.0081
0.040	0°	0.000	

using the same powder samples as in the work reported here. The resulting spectra, however, were very complex and it would be extremely difficult to obtain any quantitative information from them due to the fact that spin reorientations depend on the orientation of the particular crystallite in the applied field. All that was concluded from these spectra was that, for $c \leq 0.04$, the applied field did induce spin reorientations. Quantitative information would require the use of single-crystal samples. Single crystals would also enable the absolute direction of the hyperfine field to be measured directly in zero applied field.

ACKNOWLEDGMENTS

This work was supported by the National Research Council of Canada under Grant No. A2275. It is a pleasure for one of us (D. C. P.) to acknowledge the support of Professor C. E. Johnson while this paper was being written and to thank Dr. A. N. Buckley and Dr. J. M. D. Coey for useful discussions during the early stages of this work.

---

*Present address: Department of Physics, University of Liverpool, Liverpool, U. K.

[1]I. Maartense, Phys. Rev. 188, 924 (1969).

[2]I. Maartense, Phys. Rev. B 6, 4324 (1972) (hereinafter referred to as I).

[3]R. W. G. Wyckoff, *Crystal Structures* (Wiley, New York, 1964).

[4]I. Dzyaloshinsky, J. Phys. Chem. Solids 4, 241 (1958); T. Moriya, Phys. Rev. 120, 91 (1960).

[5]J. Kanamori, Prog. Theor. Phys. 20, 890 (1958).

[6]A. Okiji and J. Kanamori, J. Phys. Soc. Jap. 19, 908 (1964); K. Ono and A. Ito, J. Phys. Soc. Jap. 19, 899 (1964).

[7]B. Bleaney and K. W. H. Stevens, Rep. Prog. Phys. 16, 108 (1953).

[8]A. Abragam and M. H. L. Pryce, Proc. Roy. Soc. 205, 135 (1951).

[9]K. W. H. Stevens, Proc. Phys. Soc. Lond. A 65, 209 (1952).

[10]H. N. Ok, Phys. Rev. 185, 472 (1969).

[11]F. Varret, H. Czeskleba, F. Hartmann-Boutron, and P. Imbert, J. Phys. (Paris) 33, 549 (1972).

[12]R. Ingalls, Phys. Rev. 133, A 787 (1964).

[13]H. N. Ok and J. G. Mullen, Phys. Rev. 168, 563 (1968).

[14]Y. Hazony, Phys. Rev. B 3, 711 (1971).

[15]T. M. Holden, E. C. Svensson, and P. Martel, Can. J. Phys. 50, 687 (1972).

[16]H. J. Fink and D. Shaltiel, Phys. Rev. 130, 627 (1963).

[17]B. Y. Kotyuzhanskii, Zh. Eksp. Teor. Fiz. 59, 1562 (1970) [Sov. Phys.-JETP 32, 854 (1971)].

[18]W. Marshall and C. E. Johnson, J. Phys. Radium 23, 733 (1962).

[19]C. E. Johnson, Proc. Phys. Soc. (Lond.) 92, 748 (1967).

[20]R. E. Watson and A. J. Freeman, Phys. Rev. 123, 2027 (1961).

[21]For example, R. L. Collins, and J. C. Travis, Mössbauer Effect Methodology 3, 123 (1968).

[22]C. E. Johnson in *Hyperfine Structure and Nuclear Radiations*, edited by E. Matthias and D. A. Shirley (North-Holland, Amsterdam, 1968).

[23]A. J. Freeman and R. E. Watson, Phys. Rev. 131, 2566 (1963).

[24]R. S. Preston, S. S. Hanna, and J. Heberle, Phys. Rev. 128, 2207 (1962).

[25]W. Kündig, Nucl. Instr. Meth. 48, 219 (1967).

[26]I. S. Jacobs, J. Appl. Phys. 34, 1106 (1963).